Article

Global Analysis of Bioclimatic Controls on Ecosystem Productivity Using Satellite Observations of Solar-Induced Chlorophyll Fluorescence

Nima Madani [1,2,*], John S. Kimball [1,2], Lucas A. Jones [1,2], Nicholas C. Parazoo [3] and Kaiyu Guan [4]

[1]   Numerical Terradynamic Simulation Group, College of Forestry & Conservation, University of Montana, Missoula, MT 59812, USA; johnk@ntsg.umt.edu (J.S.K.); lucas@ntsg.umt.edu (L.A.J.)
[2]   Department of Ecosystem and Conservation Sciences, College of Forestry & Conservation, University of Montana, Missoula, MT 59812, USA
[3]   Jet Propulsion Laboratory, 4800 Oak Grove Drive, Mail Stop 200-233, Pasadena, CA 91109, USA; Nicholas.C.Parazoo@jpl.nasa.gov
[4]   Department of Natural Resources and Environmental Sciences and National Center for Supercomputing Applications, University of Illinois at Urbana-Champaign, Urbana, IL 61801, USA; kaiyug@illinois.edu
*   Correspondence: nima.madani@ntsg.umt.edu

Abstract: Ecosystem productivity models rely on regional climatic information to estimate temperature and moisture constraints influencing plant growth. However, the productivity response to these environmental factors is uncertain at the global scale and has largely been defined using limited observations from sparse monitoring sites, including carbon flux towers. Recent studies have shown that satellite observations of Solar-Induced chlorophyll Fluorescence (SIF) are highly correlated with ecosystem Gross Primary Productivity (GPP). Here, we use a relatively long-term global SIF observational record from the Global Ozone Monitoring Experiment-2 (GOME-2) sensors to investigate the relationships between SIF, used as a proxy for GPP, and selected bio-climatic factors constraining plant growth at the global scale. We compared the satellite SIF retrievals with collocated GPP observations from a global network of tower carbon flux monitoring sites and surface meteorological data from model reanalysis, including soil moisture, Vapor Pressure Deficit (VPD), and minimum daily air temperature (Tmin). We found strong correspondence ($R^2 > 80\%$) between SIF and GPP monthly climatologies for tower sites characterized by mixed, deciduous broadleaf, evergreen needleleaf forests, and croplands. For other land cover types including savanna, shrubland, and evergreen broadleaf forest, SIF showed significant but higher variability in correlations between sites. In order to analyze temperature and moisture related effects on ecosystem productivity, we divided SIF by photosynthetically active radiation (SIF_p) and examined partial correlations between SIF_p and the climatic factors across a global range of flux tower sites, and over broader regional and global extents. We found that productivity in arid ecosystems is more strongly controlled by soil water content to an extent that soil moisture explains a higher proportion of the seasonal cycle in productivity than VPD. At the global scale, ecosystem productivity is affected by joint climatic constraint factors so that VPD, Tmin, and soil moisture were significant ($p < 0.05$) controls over 60, 59, and 35 percent of the global domain, respectively. Our study identifies and confirms dominant climate control factors influencing productivity at the global scale indicated from satellite SIF observations. The results are generally consistent with climate response characteristics indicated from sparse global tower observations, while providing more extensive coverage for verifying and refining global carbon and climate model assumptions and predictions.

Keywords: ecosystem productivity; FLUXNET; GPP; MODIS-MOD17; phenology; SIF; SMAP-L4C

1. Introduction

Satellite observations have been used for studying global vegetation growth and seasonal phenology, ranging from the use of vegetation greenness indices from optical-infrared (IR) sensors to monitor photosynthetic canopy cover [1–4] to vegetation optical depth and backscatter retrievals from microwave sensors to monitor canopy biomass changes [5,6]. In addition to remote sensing of canopy physical properties, bio-climatic indices related to light, temperature, and water-related environmental constraints to plant photosynthesis have also been used to predict vegetation growth and phenology metrics including growing season timing and length [7–9]. These climate indices, in conjunction with satellite observations of the vegetation Fraction of Photosynthetically Active Radiation (FPAR) and other environmental inputs, have been used in process based models for estimating vegetation Gross Primary Productivity (GPP) [10–12]. GPP is a fundamental indicator of ecosystem productivity and the primary conduit for atmosphere carbon (CO_2) uptake and sequestration through plant photosynthesis. Remote sensing vegetation indices alone are unable to directly measure GPP, instead requiring the use of models driven by environmental constraint factors such as daily minimum temperature (Tmin), Vapor Pressure Deficit (VPD), and soil moisture (SM) for indirectly estimating and monitoring GPP spatial and temporal variability [10,11].

Bioclimatic indices are an important component of Light Use Efficiency (LUE) based ecosystem productivity models [10,13] and other land surface models [14]. These models use bioclimatic indices to characterize the effect of environmental factors influencing plant photosynthesis and the net ecosystem carbon flux. A well-known satellite LUE model product, the National Aeronautics and Space Administration (NASA) Moderate Resolution Imaging Spectroradiometer (MODIS) MOD17, uses only VPD and Tmin to represent moisture and temperature related controls on GPP. The Terrestrial Carbon Flux (TCF) model [11] underpins the NASA Soil Moisture Active Passive Level 4 Carbon product (SMAP-L4C) [15], which provides regular global daily assessments of terrestrial carbon fluxes, including GPP, and uses multi-sensor satellite observations and other operational data as primary inputs. The TCF model uses a LUE approach driven by VPD and SM inputs that define respective atmospheric moisture demand and soil water supply constraints to GPP, while Tmin is used to define low temperature constraints to growth. In these LUE models, the global representation of bioclimatic factors influencing productivity has largely been derived empirically using a limited number of globally distributed carbon (CO_2) flux towers [7,16–18]. The effectiveness of this approach is limited by the number of available tower sites needed to parameterize and verify model defined response characteristics for different biomes and plant functional types, which can be a major source of model uncertainty [19,20].

The LUE approach for global operational modeling of GPP from NASA satellites was originally developed in the 1990s [21], while recent enhancements include improved calibration, finer spatial resolution observations, and representation of additional environmental controls on vegetation growth [22]. Attempts have also been made to represent spatial heterogeneity in plant functional traits influencing LUE and GPP within coarser biome type classifications [20,23]. These model enhancements have benefitted from an increase in the number of tower monitoring sites, though the available tower network is still very sparse over much of the globe [24].

Recent developments in satellite remote sensing include global observations of solar-induced canopy fluorescence (SIF). The SIF retrieval represents electromagnetic energy emitted in the 650–800 nm spectral range during plant photosynthesis [25], which has been shown to be proportional to GPP estimated from tower carbon flux measurements representing major global biomes [26–30]. Approximately 1–2% of total photosynthetically active radiation (PAR) absorbed by the canopy is emitted as SIF [31], which has been found to have stronger correspondence with GPP than satellite vegetation greenness indices [26,32]. SIF is also positively related to LUE [29], and is expected to be sensitive to bioclimatic constraints influencing plant photosynthetic activity. However, a large sensor footprint and coarse temporal compositing of the satellite SIF observations is generally needed to enhance sensor signal-to-noise, which constrains capabilities for finer landscape assessments. Despite this limitation, the satellite

SIF record provides a close observational analog for GPP. SIF may also provide an effective global observational benchmark for evaluating bioclimatic factors influencing vegetation growth and for verifying LUE model parameterizations of these processes for improving GPP estimation accuracy and performance [33].

To achieve the goal of documenting the bioclimatic factors and response patterns influencing ecosystem productivity from the perspective of the global SIF observation record, we examined moisture and temperature related controls influencing ecosystem productivity using global satellite based SIF observations as a surrogate for GPP. A multi-scale analysis was used to investigate bioclimatic factors influencing spatial and seasonal patterns in vegetation growth. The analysis included comparisons between satellite SIF and stand level GPP observations from tower sites representing major global biomes; seasonal assessments of SIF and selected bioclimatic factors for individual sub-regions, and a global analysis of predominant bioclimatic control patterns influencing productivity. We also compared global productivity response relationships indicated from the satellite SIF record against prescribed LUE model parameterized relationships developed from sparse tower observations. Regression analysis was used to assess relationships between SIF and GPP, and selected meteorological variables frequently used in LUE models to define moisture and temperature related controls to GPP, including VPD, Tmin, and surface to root zone (1m depth) soil moisture (SM). A generalized additive model was used to define the best-fit curvilinear relationships between SIF and underlying environmental constraints at the global scale.

2. Data and Methods

2.1. Datasets

Consistent global SIF observations have been acquired since 2007 from the GOME-2 sensor, onboard the European Organisation for the Exploitation of Meteorological Satellites (EUMETSAT) Meteorological Operational Satellites. The GOME-2 sensor includes four spectral channels ranging from 240–790 nm, while channel four covers the SIF sensitive spectral region from 590–790 nm [25,34] with an over-pass time of 9:30 a.m., near the peak of daily photosynthetic activity [35]. We used an existing GOME-2 SIF (version 2.6 MetOp-A) global record composited to a monthly time step and mapped to a 0.5 degree resolution global grid and WGS 1984 coordinate system [28,34]. The 2007–2015 SIF record was used to create a monthly SIF ($Mw\ m^{-2}\ sr^{-1}\ nm^{-1}$) climatology by averaging nine values for each month ($Mw\ m^{-2}\ sr^{-1}\ nm^{-1}$) for each 0.5-degree grid cell over the global domain. All the negative SIF values mostly over the water bodies were treated as no data value. The global domain for this study encompassed all land areas except for regions with sparsely vegetated cover defined by a MODIS IGBP land cover classification [36]. The resulting monthly SIF observations were compared with collocated GPP observations obtained from local scale (~1 km^2 footprint) tower carbon flux measurements representing a range of global biomes.

Satellite based Photosynthetically Active Radiation (PAR) observations from the Cloud and Earth Radiant Energy System (CERES, Ed3A) database [37] were used to account for the influence of solar radiation on the 2007–2015 GOME-2 SIF record; the CERES database is derived from MODIS observations from the Terra and Aqua satellites and has 1-degree spatial resolution and monthly averaged temporal coverage. The CERES PAR data were resampled to the same 0.5 resolution and projection format as the SIF record using nearest-neighbor resampling, and then temporally averaged to produce a monthly climatology. We then divided the SIF monthly climatology for each grid cell by the corresponding monthly mean PAR observations from CERES (Wm^{-2}). The resulting PAR-adjusted SIF metric (SIF$_P$) was used to distinguish temperature and moisture related controls on productivity apart from solar radiation. The SIF$_P$ observations were compared with mean monthly climate variables obtained from global reanalysis data for selected tower site locations and over the larger global domain. The monthly SIF$_P$ grid cells were also spatially averaged and compared with similarly averaged monthly climate variables for selected global sub-regions (Figure 1).

We used in situ GPP records from 67 global carbon flux tower sites to evaluate relationships between the stand level tower GPP observations and coarser productivity and climate controls defined from the satellite SIF observations and global reanalysis data. The tower site records were selected from the 2015 FLUXNET synthesis [38] on the basis of representing major global biomes (Figure 1), and having multi-year daily GPP records occurring after year 2007 to overlap with the GOME-2 SIF record; the resulting tower sites selected for this investigation are summarized in Table S1. Gap-filled daily tower data derived using seven different nighttime carbon flux partitioning methods [39] were averaged to create a GPP mean monthly climatology for each tower site.

We used a global daily surface meteorology record for the 2007–2015 period obtained from the Modern-Era Retrospective analysis for Research and Applications, Version 2 (MERRA2) global reanalysis [40]. The MERRA2 meteorological parameters processed for this study included daily minimum and mean air temperatures, dew point temperature, and root zone (integrated 0–1 m depth) SM. The MERRA2 data were resampled from a native 0.5×0.65-degree global grid into a 0.5-degree resolution geographic projection consistent with the GOME-2 SIF record. Atmosphere VPD was derived from the daily air temperature and dew point data [41]. The daily meteorological parameters were then averaged for each 0.5 grid cell to create a monthly climatology from the 2007–2015 MERRA2 record. The resulting VPD, Tmin, and SM monthly climatologies were used to investigate associated ecosystem bioclimatic constraints to productivity for individual tower locations and sub-regions, and the global domain following the same methods was used for SIF processing.
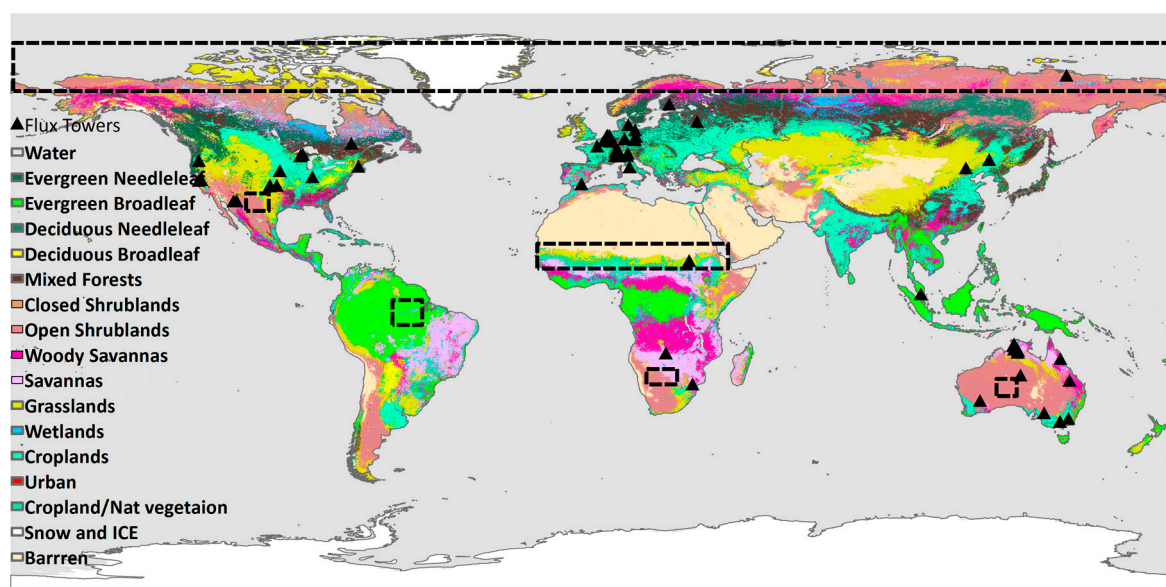

Figure 1. Location of carbon flux tower sites used for comparison with GOME-2 SIF and MERRA2 data records. Background land cover map represents IGBP land cover types from the MODIS MCD12Q1 [36] land cover product. Dashed lines denote selected sub-regions used for evaluating spatially aggregated relationships between PAR-adjusted SIF (SIF$_P$) and underlying moisture and temperature control factors influencing productivity.

2.2. Data Analysis

Linear regression analysis and the coefficient of determination (R^2) metric were used to quantify relationships between tower GPP and GOME2 SIF monthly climatology records ($n = 12$) at each tower location. Regression analysis and the Spearman correlation metric (*r*-value) were used to quantify the sign and strength of the relationships between SIF$_P$ and collocated Tmin, VPD, and SM records from MERRA2; here, regression analysis was used to evaluate relationships between SIF$_P$ and each climate variable while accounting for the influence of other covariates on the regression relationship.

A climate aridity index (AI), defined as the ratio of annual precipitation to potential evapotranspiration (P/PET) [42], was used to characterize general climate aridity over the global domain. The AI follows United Nations Environmental Program (UNEP) defined aridity categories [36], including hyperarid (AI < 0.03), arid (0.03 < AI < 0.20), semi-arid (0.20 < AI < 0.5), sub-humid (0.50 < AI <0.65), and humid (AI > 0.65) categories. Partial correlations were determined between SIF_P and each climate variable for each tower site. The tower site results were then analyzed in two-dimensional climate space defined by the global AI and mean annual temperature distributions. The resulting relationships were assessed using a 95% ($p < 0.05$) significance threshold.

An analysis was conducted to identify the pattern of influence and relative impact of each climate variable in explaining spatial and seasonal variations in vegetation growth. Partial correlations were analyzed between SIF_P and the monthly climate variables for each global grid cell. The monthly SIF_P and climate variables were also spatially aggregated and analyzed for selected global sub-regions, including northern arctic, southern USA, southern Africa, African Sahel, eastern Amazonia, and central Australia (Figure 1).

A generalized additive model [43] was used to define the smoothed curvilinear relationships between SIF_P and each climate variable from the global record. The resulting productivity response to each climate variable indicated from the SIF_P record was then compared with prescribed parameterizations of these response characteristics defined in the SMAP-L4C model product [15]. The SMAP-L4C global product is produced operationally using a satellite data driven LUE model to estimate daily GPP using MODIS vegetation and SMAP derived soil moisture observations as primary model drivers. The L4C model incorporates daily SM, VPD, and Tmin to define environmental reductions in LUE from prescribed optimal rates due to low soil moisture levels, excessive atmosphere moisture deficits, and cold temperatures. The LUE reduction is defined as the product of dimensionless environmental constraint factors ranging from 1 (no constraint) to 0 (fully constrained). Daily surface meteorological inputs to the L4C model are derived using a similar GEOS-5 land model as MERRA2, while the L4C response functions are calibrated from historical tower site observations representing major global biomes and plant functional types. All analyses were conducted in the R programing environment [44].

3. Results and Discussion

3.1. SIF, GPP, and Climatic Factors at the Tower Scale

The GOME-2 SIF global climatology shows large spatial variability in seasonal cycles congruent with general climate and latitudinal variations, indicating the influence of underlying environmental controls on vegetation phenology and productivity (Figure 2). In the northern hemisphere, a relatively abrupt and persistent SIF increase in early spring indicates the start of the growing season, consistent with a relaxation of cold temperature constraints to growth following winter dormancy [26]. The start and end of the growing season observed by satellite SIF is consistent with local flux carbon tower measurements and also different from the traditional vegetation indices, including MODIS [26]. We also note that the SIF data distinguish northern hemisphere cropland patterns and seasonality that are also different from traditional vegetation indices records [27,35]. The SIF record also shows a large seasonal amplitude and distinctive growing season over extratropical regions consistent with characteristic seasonal variations in daylength, and suitable temperature and moisture conditions for growth [45]. The SIF record shows a relatively small but distinct seasonality in the tropics, which is larger in sub-tropical savanna and grassland ecosystems, consistent with a regional gradient in water-related environmental constraints to productivity [46,47]. To investigate and clarify relationships between SIF, GPP, and underlying environmental control factors at the stand level, we compared the SIF monthly climatology with corresponding GPP observations from selected tower sites representing a range of global climate and land cover types (Table 1).
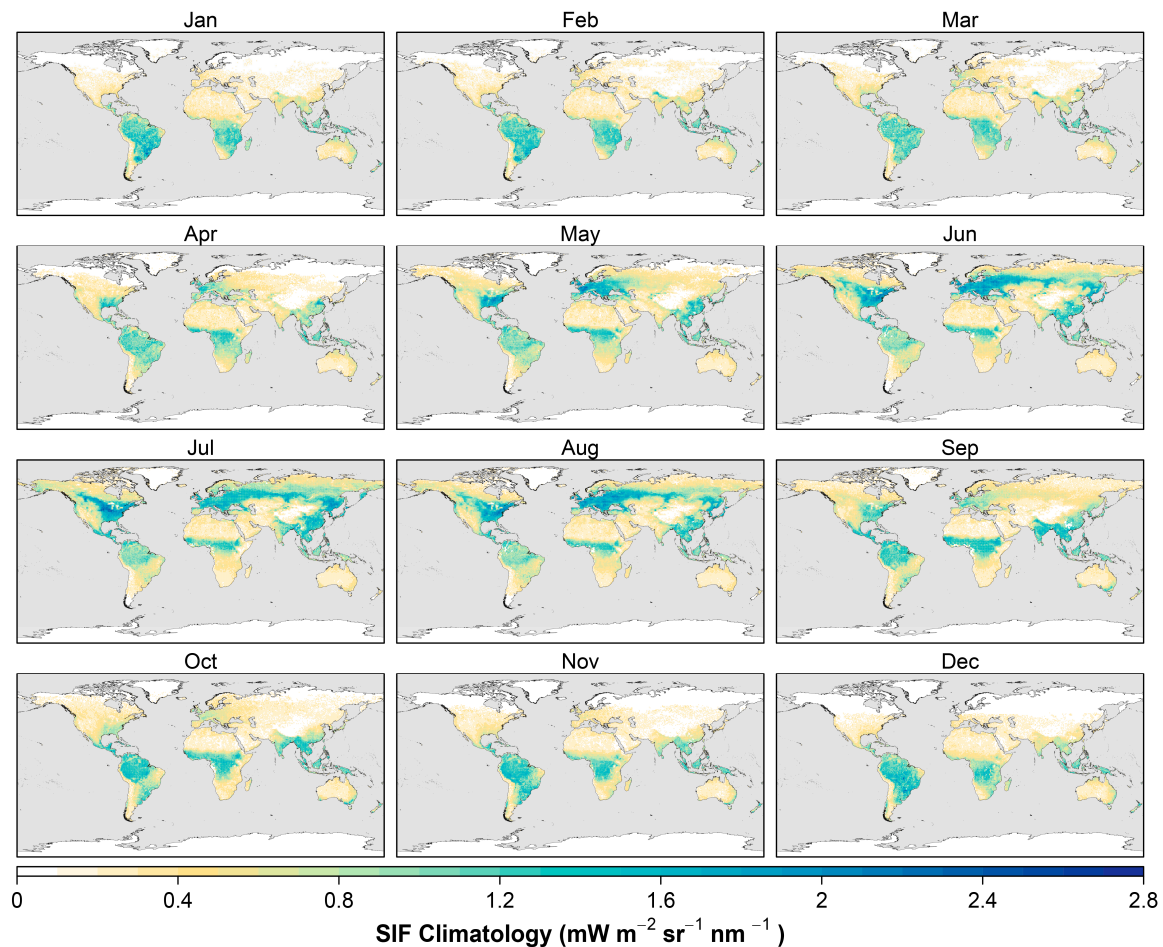
Figure 2. Global monthly SIF climatology derived from the GOME-2 satellite record from 2007–2015.

Table 1. Average and standard deviation (SD) in correspondence (R^2) between GOME-2 SIF and collocated tower GPP observations (SIF.GPP) with annual air temperature and climate aridity (AI) information for 67 tower sites stratified by their IGBP land cover class, including: EBF (Evergreen Broadleaf Forest); ENF (Evergreen Needleleaf Forest); DBF (Deciduous Broadleaf Forest); MF (Mixed Forest); OSH (Open Shrubland); WSA (Woody Savanna); SAV (Savanna); GRA (Grassland); WET (Wetland) and CRO (Cropland).

IGBP	No. of Sites	Mean Annual Temp (°C)	AI (P/PET)	SIF.GPP (R^2; %)
EBF	3	17 ± 7	1.07 ± 0.4	50 ± 32
ENF	11	8 ± 7	1.13 ± 0.4	83 ± 17
DBF	8	11 ± 6	0.98 ± 0.2	87 ± 12
MF	4	7 ± 3	1.18 ± 0.2	90 ± 16
OSH	3	4 ± 16	0.45 ± 0.2	59 ± 41
WSA	4	22 ± 6	0.50 ± 0.1	79 ± 15
SAV	6	23 ± 5	0.33 ± 0.2	62 ± 37
GRA	16	11 ± 7	1.04 ± 0.8	76 ± 27
WET	4	12 ± 11	0.85 ± 0.1	78 ± 14
CRO	8	11 ± 3	0.83 ± 0.3	82 ± 15

The tower site comparisons showed statistically significant correspondence ($p < 0.05$) between the SIF and GPP observations at most sites, except for two low productivity grassland and savanna sites in Australia where the average GPP was less than 2 g C m^{-2} day^{-1}. On average, the SIF and GPP correspondence was strongest for mixed forests, followed by deciduous broadleaf and evergreen

needleleaf forests, and cropland sites ($R^2 > 80\%$). SIF and tower GPP correspondence was lower, but still significant for the evergreen broadleaf forest (EBF) sites ($R^2 = 50\%$). The weaker SIF and GPP correspondence at lower productivity and tropical EBF sites may reflect greater SIF uncertainty for sparsely vegetated, low productivity sites [48] and tropical rainforest sites characterized by persistent cloud cover [28]. On the other hand, weak vertical mixing of CO_2 during the nighttime, especially in tropical forests [49,50], may be a source of uncertainty in flux tower GPP derived using model based gap filling methods. Relatively weak regression relationships in wet tropical forest areas may also be an artifact of lower characteristic seasonal climate variability in these areas. Overall, the significant and relatively strong correspondence between the SIF and tower GPP observations representing major land cover types and biomes is consistent with previous studies showing that SIF is proportional to GPP [26–30,33].

The partial correlations between the PAR adjusted SIF records (SIF_P) and selected MERRA2 climate variables (VPD, Tmin, SM) at the tower site locations are plotted in two-dimensional climate space defined by mean annual temperature and climate aridity (AI) along with temperature and AI conditions for all other grid cells within the global domain (Figure 3). Box plots showing the spatial distributions of tower SIF_P and climate correlations by land cover class are also shown. Most of the moisture-limited sites are located in regions with mean annual temperatures above 20 °C, with low precipitation and high potential evapotranspiration (AI < 0.5); the moisture limitations to SIF_P at these sites were generally represented by respective inverse or direct correlations with VPD and SM. However, the SIF_P and SM relationships were highly variable among tower sites. Soil moisture was directly correlated with SIF_P for semi-arid (0.2 < AI < 0.5) savanna (SAV) and woody savanna (WSA) sites, with average correlations of 0.61 and 0.48, respectively. In contrast, relatively humid climate sites (AI > 0.9), including forest (EBF, DBF, ENF, MF) and cropland (CRO) towers, show predominantly inverse correlations with soil moisture. The weaker correlation between SIF_P and soil moisture in forest ecosystems is consistent with reduced water supply restrictions supporting greater vegetation growth in wetter climates. The reduced SM dependence in forests may also reflect characteristic deeper rooting depths for trees [51] and additional water storage capacity in woody biomass beyond root zone soil moisture. The relationship between SIF_P and soil moisture is highly variable for open shrubland (OSH), grassland (GRA), and wetland (WET) sites, including both the sign and strength of correlations; these land cover types also showed a large diversity in temperature and moisture conditions. For example, open shrubland covers much of central Australia and is characterized by a warm and dry climate (AI < 0.5) where SIF_P is directly proportional to SM. In contrast, a major portion of northern taiga and tundra is also characterized as OSH, but with a much colder climate, where SIF_P is more strongly correlated with Tmin. The relatively strong SIF_P correlations with SM for arid sites also suggests that soil moisture imposes additional constraints on productivity beyond VPD, and that including soil moisture as an additional control in productivity models may enhance model GPP estimates in arid regions.

The SAV and WSA sites showed a negative relationship between SIF_P and VPD, but the correlation was 17% weaker than the relationship between SIF_P and SM. Tower sites in colder climate areas generally showed a positive correlation with VPD. Among the EBF sites analyzed, the tropical rain forest site showed positive SIF_P correlations with both VPD and Tmin, consistent with minimal moisture constraints to plant growth and the near-exponential relationship between temperature and atmosphere moisture holding capacity. Other EBF sites located in more arid regions showed a negative SIF_P relationship with VPD and Tmin.

Among the land cover types examined, the MF, ENF, and DBF sites showed the strongest correlations with minimum temperature. These forest sites were generally located in northern hemisphere temperate and boreal climate zones with lower mean annual temperatures and where plant productivity has large characteristic seasonality ranging between winter lows with strong cold temperature constraints on biological processes, to active growth conditions under warmer temperatures in spring and summer. Overall, these results indicate that SIF is not only proportional to vegetation productivity, but also reflects the effects of seasonal moisture and temperature constraints on photosynthetic activity.
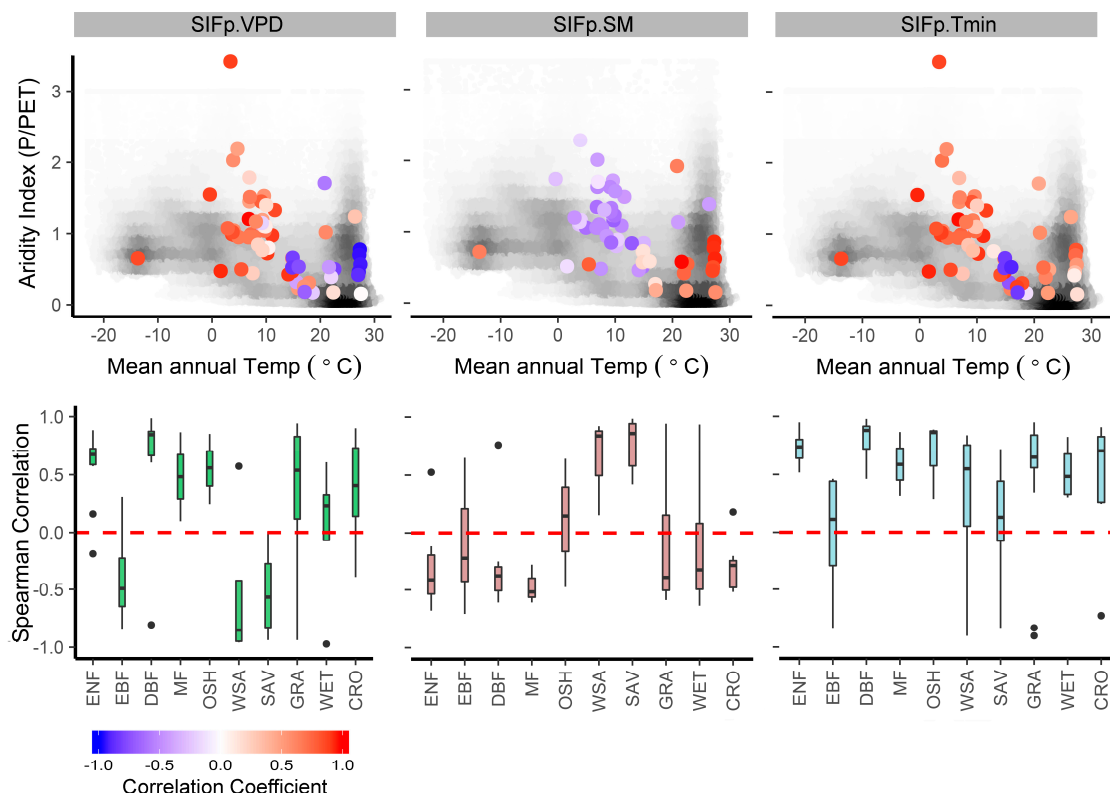
Figure 3. Partial correlations between SIF_P and moisture and temperature variables affecting productivity (VPD, SM, Tmin) for selected global carbon flux tower sites. The Spearman correlation coefficients for each tower site are superimposed on global climate space defined by mean annual temperature and climate aridity (AI). The AI and annual temperature distributions of all grid cells within the global domain are also plotted, where darker and lighter shading denotes respective higher and lower cell densities. The boxplots show the spatial variability in tower site SIF_P correlations for VPD (SIF_P.VPD), SM (SIF_P.SM), and Tmin (SIF_P.Tmin) by land cover class. Only tower sites with statistically significant correlations ($p < 0.05$) were used in the analysis (2, 6, and 3 sites did not show statistically significant correlation with VPD, SM, and Tmin, respectively).

3.2. Regional Scale Analysis of Bioclimatic Factors

We analyzed partial correlations between spatially averaged monthly SIF_P and climate records within six sub-regions (Figure 1) representing a range of global climate and land cover diversity. The partial correlation results for the six sub-regions are presented in Figure 4. The AI was used to show the proportional area of each region characterized by different climate aridity categories [52]. The direction and strength of the correlations between SIF_P and the different climate variables for each sub-region varied in accordance with regional differences in vegetation and climate conditions, consistent with the tower site results. The SIF_P.SM relationship is congruent with climate aridity and showed direct correspondence in dry biomes, inverse relationships in humid biomes, and intermediate $(+/−)$ correlations in areas with a seasonal dry climate. In Arctic tundra, characterized by an extended winter cold season, SIF_P follows Tmin and VPD seasonal cycles, but it is inversely correlated with SM. In central Australia, which has a relatively warm and arid climate, SIF_P follows the seasonal cycle in SM and shows inverse and relatively weak correlations with VPD and Tmin, despite having similar IGBP land cover conditions as tundra. In the southern US, which has a predominantly semi-arid climate, SIF_P is significantly correlated with multiple climate variables, but is directly proportional to soil moisture during the growing season. In the semi-arid African Sahel, soil moisture has a dominant influence on SIF_P and is the most significant variable controlling productivity. SIF_P has a positive but relatively weak correlation with Tmin and a negative correlation with VPD, which is of secondary importance after

soil moisture in influencing productivity in the Sahel. In southern Africa, which is also predominantly semi-arid, productivity is still strongly and directly proportional to soil moisture, while the other climate variables have a significant but weaker influence on productivity. In eastern Amazonia, SIF_P shows enhanced productivity from July to October, consistent with increasing photosynthetic activity during the dry season [53,54]; in this humid tropical region, SIF_P is directly proportional to VPD and negatively correlated with SM and Tmin.
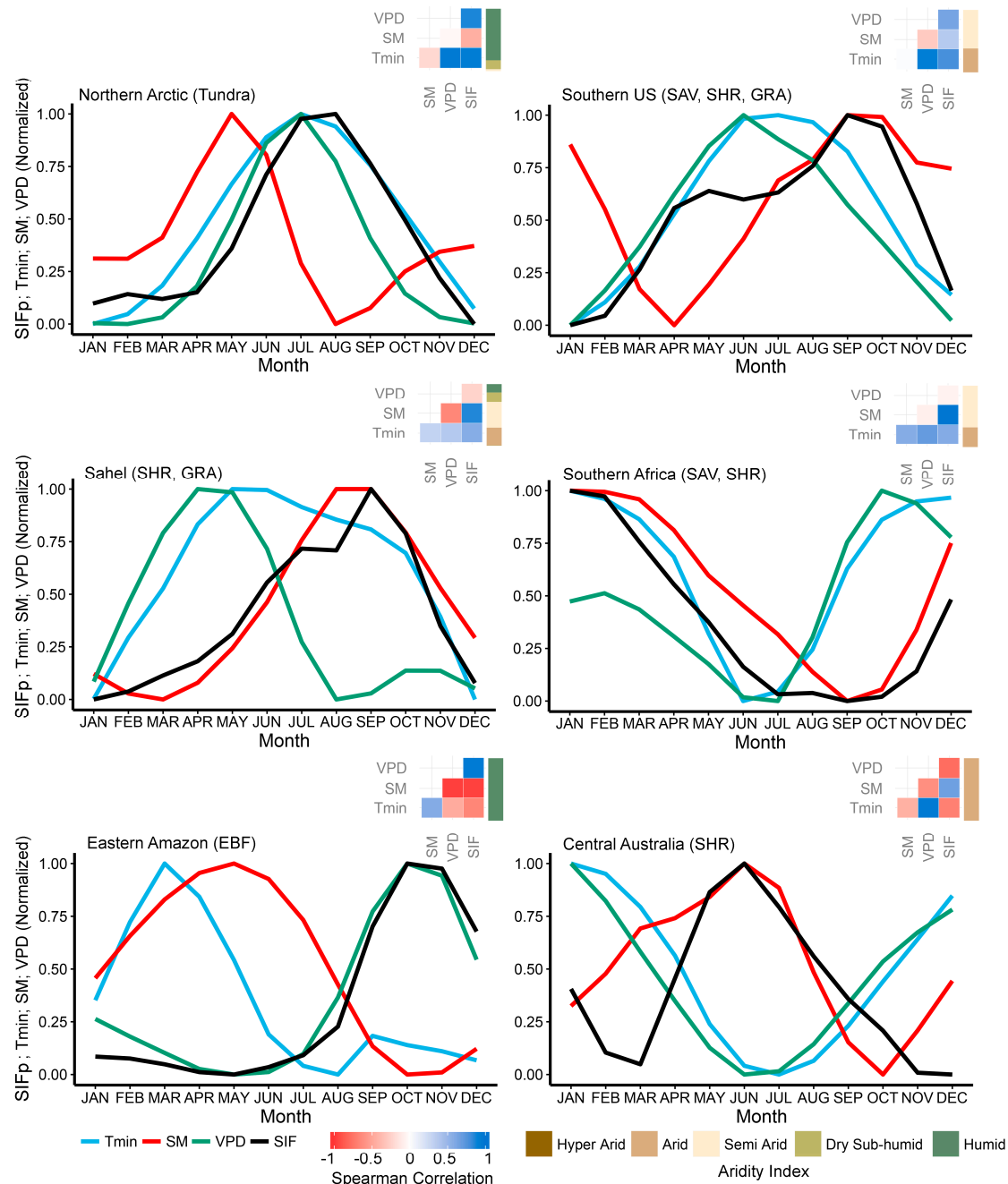
Figure 4. Monthly variability in SIF_P and associated climate variables for VPD, SM, and Tmin for the selected global sub-regions. The dominant IGBP land cover categories within each sub-region are also shown. Annotations show the partial correlation matrix between SIF_P and the different climate variables. The AI annotations show the relative proportion of different climate aridity categories in each sub-region.

3.3. Climatic Factors at the Global Scale

The global analysis of monthly climatology relationships reveals significant SIF$_P$ correlations with VPD, Tmin, and SM over approximately 60, 59, and 35 percent of the global domain, respectively (Figure 5). In many areas, SIF$_P$ was significantly correlated with more than one climate variable. In most northern temperate, boreal, and Arctic ecosystems, Tmin had a dominant influence on productivity consistent with a shorter growing season and colder mean annual temperatures at higher latitudes. VPD had a secondary and positive influence on SIF$_P$ in these areas due to the large seasonal temperature cycle at higher latitudes and close relationship between temperature and VPD. VPD and Tmin had primary and secondary influences on SIF$_P$ in wet tropical areas, with a general tendency toward greater VPD control in wetter tropical areas of Southeast Asia relative to the African Congo and Amazonia, which have relatively longer dry cycles [46]. The larger VPD influence on SIF$_P$ in wet tropical areas is consistent with the direct role of the atmospheric moisture deficit in driving water movement through the soil-plant-atmosphere system via evapotranspiration, and by consequence canopy-atmosphere CO_2 exchange, when water supply is non-limiting. However, the correlations were relatively weak due to the characteristic smaller seasonal climate cycle in the tropics.

Soil moisture had a dominant influence on SIF$_P$ over arid climate zones and other areas with marked seasonal dry cycles, including the southwest US, east Africa, southern Eurasia, the Indian subcontinent, and central Australia. In Australia, soil moisture was the dominant control on SIF$_P$. In Africa, soil moisture was a dominant control on productivity over 15.7% more area than VPD. The global patterns in relative influence of the different climate factors on SIF$_P$ are also consistent with the tower site (Figure 2) and aggregated regional summaries (Figure 3). These results confirm the importance of soil moisture related water supply controls on productivity in addition to atmospheric moisture demand constraints represented by VPD, particularly in semi-arid and arid climate zones extending over more than 30 percent of the global domain.
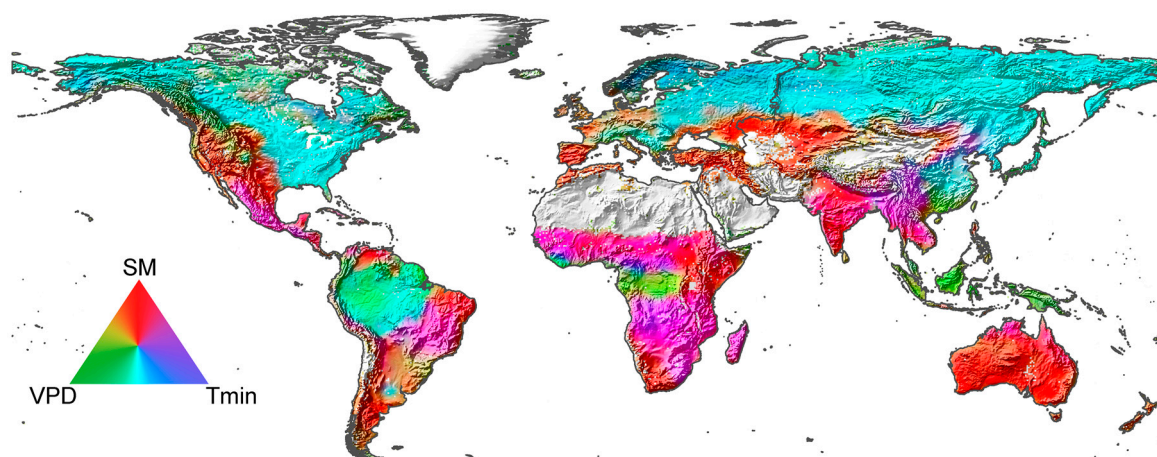

Figure 5. The Red-Green-Blue (RGB) map showing the global pattern of relative influence of the three bioclimatic control variables on ecosystem productivity derived from partial correlations between SIF$_P$ and VPD, SM, and Tmin monthly climatology records. Gray and white areas denote open water, barren land, and permanent ice, and snow areas are excluded from the study domain.

3.4. Comparing SIF and LUE Model Derived Bioclimatic Controls

A generalized additive model (GAM) [55] was fit to the SIF$_p$ data using each climate variable from the global record. The GAM adds smoothed non-parametric functions to the parametric part of a generalized linear model [55], allowing for greater flexibility and improved fit compared to generalized linear model [56]. A similar additive model approach was used to define the global relationship between each climate variable and the dimensionless (0–1) LUE model environmental

response metric defined from the SMAP-L4C product [15]. The LUE model response functions for Tmin, VPD, and SM are prescribed for up to eight different plant functional types using a global land cover classification and general biome properties lookup table calibrated from sparse tower observations. The additive model results capture the smoothed response curves determined from the individual monthly SIF_P and model LUE response characteristics from every 0.5 degree grid cell within the global domain as defined from the MERRA2 climate record.

The resulting SIF_P and LUE model global climate response relationships are presented in Figure 6. The SIF_P results indicate that productivity is directly proportional to VPD up to a level of approximately 1000 Pa, but with a rapid productivity decline at higher VPD levels until approximately 4000 Pa; a slight positive SIF_P response to more extreme VPD levels represents a small number of arid grid cells and may reflect greater SIF uncertainty in these sparsely vegetation areas. SIF_P is directly proportional to SM until the soil water content reaches approximately 70% of saturation, followed by a small productivity decline with higher moisture levels. The apparent SIF_P decline under wet soil conditions generally occurs in northern latitude boreal and tundra wetland complexes and may reflect greater soil nutrient limitations to plant growth under characteristically colder and wetter soil conditions in these areas [57]. The global SIF_P record shows a strong positive relationship with Tmin, consistent with stronger cold temperature constraints to productivity at lower temperatures. The slope of the SIF_P and Tmin relationship is also shallower below approximately 0.0 °C, indicating slowed biological processes and reduced vegetation activity under freezing temperatures. Overall, the resulting global response curves also indicate that VPD, SM, and Tmin respectively explain 42.7, 20.2, and 41.3 percent of SIF_P variability ($p < 0.001$), respectively.
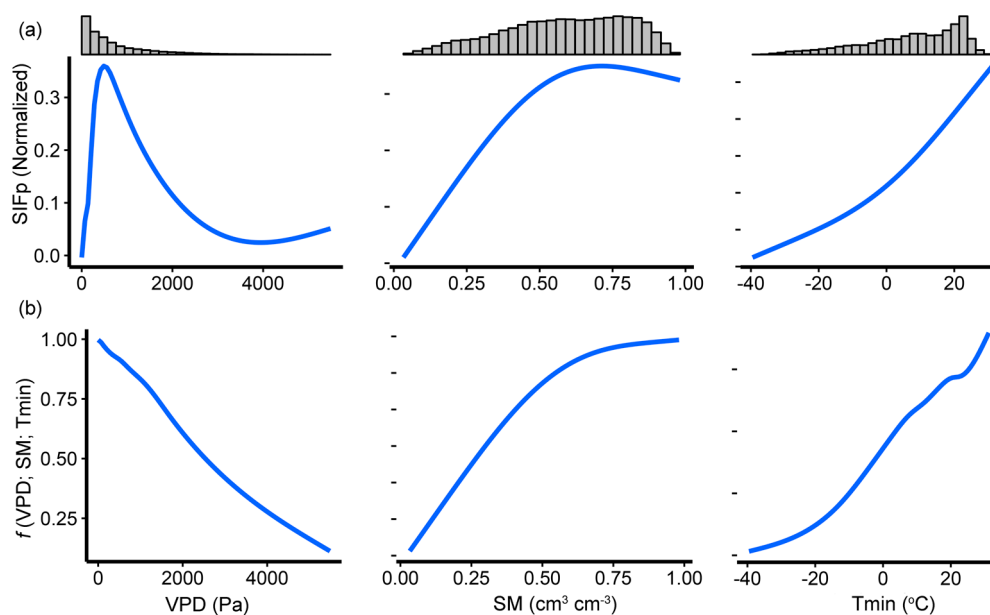

Figure 6. Global SIF_P and LUE model defined relationships with VPD, SM, and Tmin monthly climatology records; (**a**) Smoothed best-fit environmental response curves derived using a generalized additive model showing the relationship between SIF_P (*y* axis, normalized between 20th and 90th percentiles) and each climate variable (*x* axis) defined from all 0.5 degree global grid cells. Bars on the top of the plots show the relative distributions of global grid cells; (**b**) additive model best-fit environmental response curves defined from the SMAP-L4C LUE model, where the dimensionless LUE scalars range between fully constrained (0) and no constraint (1) on estimated productivity [15].

The L4C results are generally consistent with the SIF_P response characteristics (Figure 6b), confirming global model parameterizations defined from sparse tower observations. However, there were also notable differences between the SIF_P and L4C derived curves. Unlike SIF_P, the L4C results

do not show a positive productivity response to VPD under smaller humidity deficits; the lack of a positive VPD response is consistent with model LUE parameterizations that only define VPD restrictions on growth [13]. The L4C soil moisture response shows reduced sensitivity under higher soil moisture levels, but without a decreasing productivity response under wetter soil extremes. The lack of productivity decline under wet soil conditions may be due to a paucity of tower observations in wetland sites, which are needed to define model response characteristics. The greater divergence between SIF_P and L4C response characteristics generally occurs at the margins of the global distributions and reflects greater uncertainty due to a smaller population sample size and fewer available tower site observations for model parameterization.

3.5. Study Limitations and Future Directions

The methods and results from this study were constrained by several factors including the use of spatially coarse SIF and meteorological data, and global relationships defined by a monthly climatology. Our study also assumes that SIF is a linear approximation of GPP, which has been demonstrated from previous field, airborne, and satellite-based studies [28,58–60]. While our results confirm the linear correspondence between SIF and GPP for the global scale and monthly climatology examined, the mechanisms of the linear SIF-GPP relationship are still an ongoing study topic and may vary at finer spatial and temporal scales.

Improving the understanding of processes affecting relationships between SIF and GPP would be valuable for further improving vegetation productivity modeling in the context of our study. Further research is also needed to clarify the effects of temporal trends and inter-annual climate variability on ecosystem productivity. Additionally, climate parameters from global reanalysis are associated with uncertainties, while potential environmental lag effects on plant growth, and other influences beyond temperature and moisture were not addressed in this study. Nevertheless, the satellite SIF record provides the means for global verification and potential refinement of model assumptions and environmental response characteristics developed from sparse tower observations.

4. Conclusions

In this study, we conducted a global assessment of bioclimatic controls affecting ecosystem productivity using both globally comprehensive productivity observations from satellite SIF retrievals and in situ GPP observations from sparse tower sites representing a diverse set of global biomes. Moisture and temperature related controls influencing productivity were defined using VPD, SM, and Tmin from global reanalysis data. The satellite based SIF observations were adjusted by PAR (SIF_P) to distinguish temperature and moisture related controls on productivity apart from solar radiation effects. Our results show that the satellite SIF observations provide an effective proxy for ecosystem GPP and can be used with other ancillary information to clarify environmental controls driving spatial and seasonal variations in global vegetation growth. The SIF observations also provide an independent assessment and confirmation of prescribed environmental response characteristics used in global productivity model assessments.

Satellite remote sensing based vegetation greenness indices have been used to monitor global vegetation cover and productivity for more than three decades. However, satellite data driven productivity models generally require additional information to define environmental restrictions on vegetation activity and growth. The effect of bio-climatic factors on plant phenology and productivity has been empirically analyzed before, but has been limited to a relatively small number of in situ observation sites such as carbon flux towers. Our study results indicate large regional and seasonal variations in ecosystem productivity that are strongly influenced by underlying moisture and temperature related controls. Soil moisture provides effective information on water supply related controls to productivity that extend beyond atmosphere moisture demand drivers and constraints represented by VPD, particularly in drier climate zones. Our findings also suggest that despite large variability in the SIF_P response to environmental controls in different ecosystems, the mean response characteristics

indicated from the global satellite record were largely consistent with LUE model defined response characteristics used in the SMAP-L4C carbon product and defined from sparse tower observations. The satellite based SIF observations from GOME-2 were found to be an effective surrogate for GPP and sensitive to environmental factors influencing ecosystem productivity as derived from the global reanalysis data. The satellite SIF observations appear to provide an effective means for verifying model assumptions and representations of critical environmental response characteristics that may lead to better understanding and more reliable model predictions.

Author Contributions: N.M. led in the design, analysis, and writing of the paper. All authors contributed significantly to the design, writing, and revisions of the manuscript.

References

1. Jin, C.; Xiao, X.; Merbold, L.; Arneth, A.; Veenendaal, E.; Kutsch, W.L. Phenology and gross primary production of two dominant savanna woodland ecosystems in Southern Africa. *Remote Sens. Environ.* **2013**, *135*, 189–201. [CrossRef]

2. Brown, M.E.; de Beurs, K.M.; Marshall, M. Global phenological response to climate change in crop areas using satellite remote sensing of vegetation, humidity and temperature over 26 years. *Remote Sens. Environ.* **2012**, *126*, 174–183. [CrossRef]

3. Kross, A.; Fernandes, R.; Seaquist, J.; Beaubien, E. The effect of the temporal resolution of NDVI data on season onset dates and trends across Canadian broadleaf forests. *Remote Sens. Environ.* **2011**, *115*, 1564–1575. [CrossRef]

4. Zhang, X.; Friedl, M.A.; Schaaf, C.B. Global vegetation phenology from Moderate Resolution Imaging Spectroradiometer (MODIS): Evaluation of global patterns and comparison with in situ measurements. *J. Geophys. Res. Biogeosci.* **2006**, *111*, 1–14. [CrossRef]

5. Jones, M.O.; Jones, L.A.; Kimball, J.S.; McDonald, K.C. Satellite passive microwave remote sensing for monitoring global land surface phenology. *Remote Sens. Environ.* **2011**, *115*, 1102–1114. [CrossRef]

6. Guan, K.Y.; Wolf, A.; Medvigy, D.; Caylor, K.K.; Pan, M.; Wood, E.F. Seasonal coupling of canopy structure and function in African tropical forests and its environmental controls. *Ecosphere* **2013**, *4*, 1–21. [CrossRef]

7. Jolly, W.M.; Nemani, R.; Running, S.W. A generalized, bioclimatic index to predict foliar phenology in response to climate. *Glob. Chang. Biol.* **2005**, *11*, 619–632. [CrossRef]

8. Stöckli, R.; Rutishauser, T.; Baker, I.; Liniger, M.A.; Denning, S. A global reanalysis of vegetation phenology. *J. Geophys. Res.* **2011**, *116*, G03020. [CrossRef]

9. Kim, Y.; Kimball, J.S.; Zhang, K.; McDonald, K.C. Satellite detection of increasing Northern Hemisphere non-frozen seasons from 1979 to 2008: Implications for regional vegetation growth. *Remote Sens. Environ.* **2012**, *121*, 472–487. [CrossRef]

10. Running, S.W.; Nemani, R.R.; Heinsch, F.A.; Zhao, M.; Reeves, M.; Hashimoto, H. A Continuous Satellite-Derived Measure of Global Terrestrial Primary Production. *Bioscience* **2004**, *54*, 547–560. [CrossRef]

11. Kimball, J.S.; Jones, L.A.; Zhang, K.; Ke, Z.; Heinsch, F.A.; McDonald, K.C.; Oechel, W.C. A Satellite Approach to Estimate Land—Atmosphere CO_2 Exchange for Boreal and Arctic Biomes Using MODIS and AMSR-E. *IEEE Trans. Geosci. Remote Sens.* **2009**, *47*, 569–587. [CrossRef]

12. Zhao, M.; Running, S.W. Drought-induced reduction in global terrestrial net primary production from 2000 through 2009. *Science* **2010**, *329*, 940–943. [CrossRef] [PubMed]

13. Zhao, M.; Heinsch, F.A.; Nemani, R.R.; Running, S.W. Improvements of the MODIS terrestrial gross and net primary production global data set. *Remote Sens. Environ.* **2005**, *95*, 164–176. [CrossRef]

14. Levis, S.; Bonan, G.B. Simulating springtime temperature patterns in the community atmosphere model coupled to the community land model using prognostic leaf area. *J. Clim.* **2004**, *17*, 4531–4540. [CrossRef]

15. Kimball, J.; Jones, L.A.; Glassy, J.P; Reichle, R. *SMAP L4 Global Daily 9 km Carbon Net Ecosystem Exchange*; Version 2; NASA National Snow and Ice Data Center Distributed Active Archive Center: Boulder, CO, USA, 2016.

16. Foley, J.A.; Prentice, I.C.; Ramankutty, N.; Levis, S.; Pollard, D.; Sitch, S.; Haxeltine, A. An integrated biosphere model of land surface processes, terrestrial carbon balance, and vegetation dynamics. *Glob. Biogeochem. Cycles* **1996**, *10*, 603–628. [CrossRef]

17. Beer, C.; Reichstein, M.; Tomelleri, E.; Ciais, P.; Jung, M.; Carvalhais, N.; Rödenbeck, C.; Arain, M.A.; Baldocchi, D.; Bonan, G.B.; et al. Terrestrial gross carbon dioxide uptake: Global distribution and covariation with climate. *Science* **2010**, *329*, 834–838. [CrossRef] [PubMed]

18. Jung, M.; Reichstein, M.; Margolis, H.A.; Cescatti, A.; Richardson, A.D.; Arain, M.A.; Arneth, A.; Bernhofer, C.; Bonal, D.; Chen, J.; et al. Global patterns of land-atmosphere fluxes of carbon dioxide, latent heat, and sensible heat derived from eddy covariance, satellite, and meteorological observations. *J. Geophys. Res.* **2011**, *116*, 1–16. [CrossRef]

19. Turner, D.P.; Gower, S.T.; Cohen, W.B.; Gregory, M.; Maiersperger, T.K. Effects of spatial variability in light use efficiency on satellite-based NPP monitoring. *Remote Sens. Environ.* **2002**, *80*, 397–405. [CrossRef]

20. Madani, N.; Kimball, J.S.; Affleck, D.L.R.; Kattge, J.; Graham, J.; van Bodegom, P.M.; Reich, P.B.; Running, S.W. Improving ecosystem productivity modeling through spatially explicit estimation of optimal light use efficiency. *J. Geophys. Res. Biogeosci.* **2014**, *119*, 1755–1769. [CrossRef]

21. Running, S.; Baldocchi, D.; Turner, D.P.; Gower, S.T.; Bakwin, P.S.; Hibbard, K.A. A global terrestrial monitoring network integrating tower fluxes, flask sampling, ecosystem modeling and EOS satellite data. *Remote Sens. Environ.* **1999**, *127*, 108–127. [CrossRef]

22. Running, S.W.; Zhao, M. *User's Guide Daily GPP and Annual NPP (MOD17A2/A3) Products NASA Earth Observing System MODIS Land Algorithm*; The Numerical Terradynamic Simulation Group: Missoula, MT, USA, 2015.

23. Van Bodegom, P.M.; Douma, J.C.; Verheijen, L.M. A fully traits-based approach to modeling global vegetation distribution. *Proc. Natl. Acad. Sci. USA* **2014**, *111*, 13733–13738. [CrossRef] [PubMed]

24. Schimel, D.; Pavlick, R.; Fisher, J.B.; Asner, G.P.; Saatchi, S.; Townsend, P.; Miller, C.; Frankenberg, C.; Hibbard, K.; Cox, P. Observing terrestrial ecosystems and the carbon cycle from space. *Glob. Chang. Biol.* **2015**, *21*, 1762–1776. [CrossRef] [PubMed]

25. Köhler, P.; Guanter, L.; Joiner, J. A linear method for the retrieval of sun-induced chlorophyll fluorescence from GOME-2 and SCIAMACHY data. *Atmos. Meas. Tech.* **2015**, *8*, 2589–2608. [CrossRef]

26. Walther, S.; Voigt, M.; Thum, T.; Gonsamo, A.; Zhang, Y.; Koehler, P.; Jung, M.; Varlagin, A.; Guanter, L. Satellite chlorophyll fluorescence measurements reveal large-scale decoupling of photosynthesis and greenness dynamics in boreal evergreen forests. *Glob. Chang. Biol.* **2016**, *22*, 2979–2996. [CrossRef] [PubMed]

27. Guanter, L.; Zhang, Y.; Jung, M.; Joiner, J.; Voigt, M.; Berry, J.A.; Frankenberg, C.; Huete, A.R.; Zarco-Tejada, P.; Lee, J.-E.; et al. Global and time-resolved monitoring of crop photosynthesis with chlorophyll fluorescence. *Proc. Natl. Acad. Sci. USA* **2014**, *111*, E1327–E1333. [CrossRef] [PubMed]

28. Joiner, J.; Yoshida, Y.; Vasilkov, A.P.; Schaefer, K.; Jung, M.; Guanter, L.; Zhang, Y.; Garrity, S.; Middleton, E.M.; Huemmrich, K.F.; et al. The seasonal cycle of satellite chlorophyll fluorescence observations and its relationship to vegetation phenology and ecosystem atmosphere carbon exchange. *Remote Sens. Environ.* **2014**, *152*, 375–391. [CrossRef]

29. Yang, X.; Tang, J.; Mustard, J.F.; Lee, J.; Rossini, M.; Joiner, J.; Munger, J.W.; Kornfeld, A.; Richardson, A.D. Solar-induced chlorophyll fluorescence that correlates with canopy photosynthesis on diurnal and seasonal scales in a temperate deciduous forest. *Geophys. Res. Lett.* **2015**, *42*, 2977–2987. [CrossRef]

30. Joiner, J.; Yoshida, Y.; Guanter, L.; Lindstrot, R.; Voigt, M.; Jung, M.; Vasilkov, A.; Middleton, E.; Huemmrich, K.F.; Tucker, C.J.; et al. New Measurements of Chlorophyll Fluorescence with Gome-2 and Comparisons with the Seasonal Cycle of GPP from Flux Towers. In Proceedings of the 5th INT Ernational Workshop on Remote Sensing of Vegetation Fluoresce NCE, Paris, France, 22–24 April 2014; pp. 7–11.

31. Maxwell, K.; Johnson, G.N. Chlorophyll fluorescence—A practical guide. *J. Exp. Bot.* **2000**, *51*, 659–668. [CrossRef] [PubMed]

32. Wagle, P.; Zhang, Y.; Jin, C.; Xiao, X. Comparison of solar-induced chlorophyll fluorescence, light use efficiency, and process- based GPP models in maize. *Ecol. Appl.* **2016**, *26*, 1211–1222. [CrossRef] [PubMed]

33. Zhang, Y.; Xiao, X.; Jin, C.; Dong, J.; Zhou, S.; Wagle, P.; Joiner, J.; Guanter, L.; Zhang, Y.; Zhang, G.; et al. Consistency between sun-induced chlorophyll fluorescence and gross primary production of vegetation in North America. *Remote Sens. Environ.* **2016**, *183*, 154–169. [CrossRef]

34. Joiner, J.; Yoshida, Y.; Vasilkov, A.P.; Corp, L.A.; Middleton, E.M. First observations of global and seasonal terrestrial chlorophyll fluorescence from space. *Biogeosciences* **2011**, *8*, 637–651. [CrossRef]

35. Guan, K.; Lobell, D.B.; Berry, J.; Joiner, J.; Guanter, L.; Zhang, Y.; Badgley, G. Improving the mointoring of crop productivity using spaceborne solar-induced fluorescence. *Geophys. Res. Lett.* **2015**, *22*, 716–726.

36. Friedl, M.A.; Sulla-Menashe, D.; Tan, B.; Schneider, A.; Ramankutty, N.; Sibley, A.; Huang, X. MODIS Collection 5 global land cover: Algorithm refinements and characterization of new datasets. *Remote Sens. Environ.* **2010**, *114*, 168–182. [CrossRef]

37. CERES Science Team. *CERES SYN1deg Data Products: SYN1deg-M3Hour Ed3A*; NASA Atmospheric Science Data Center (ASDC): Hampton, VA, USA; 2013.

38. Oak Ridge National Laboratory Distributed Active Archive Center (ORNL DAAC). FLUXNET Web Page. ORNL DAAC: Oak Ridge, TN, USA, 2015. Available online: http://fluxnet.ornl.gov (accessed on 7 November 2016).

39. FLUXNET2015 Release—Processing Pipeline. Fluxdata, The Data Portal Serving the FLUXNET Community, 2016. Available online: http://fluxnet.fluxdata.org/data/fluxnet2015-dataset/data-processing/ (accessed on 7 November 2016).

40. Bosilovich, M.G.; Lucchesi, R.; Suarez, M. *MERRA-2: File Specification. GMAO Office Note No. 9, Version 1.0*; The Sciences Division NASA Goddard Space Flight Center: Greenbelt, MD, USA, 2015.

41. Murray, F.W. On the Computation of Saturation Vapor Pressure. *J. Appl. Meteorol.* **1967**, *6*, 203–204. [CrossRef]

42. Zomer, R.J.; Trabucco, A.; Bossio, D.A.; Verchot, L.V. Climate change mitigation: A spatial analysis of global land suitability for clean development mechanism afforestation and reforestation. *Agric. Ecosyst. Environ.* **2008**, *126*, 67–80. [CrossRef]

43. Wood, S. Generalized additive models. *Stat. Sci.* **2010**, *3*, 297–318.

44. R Core Team. *R: A Language and Environment for Statistical Computing*; R Foundation for Statistical Computing: Vienna, Austria, 2016.

45. Nemani, R.R.; Keeling, C.D.; Hashimoto, H.; Jolly, W.M.; Piper, S.C.; Tucker, C.J.; Myneni, R.B.; Running, S.W. Climate-driven increases in global terrestrial net primary production from 1982 to 1999. *Science* **2003**, *300*, 1560–1563. [CrossRef] [PubMed]

46. Guan, K.; Pan, M.; Li, H.; Wolf, A.; Wu, J.; Medvigy, D.; Caylor, K.K.; She, J.; Wood, E.F.; Malhi, Y.; et al. Photosynthetic seasonality of global tropical forests constrained by hydroclimate. *Nat. Geosci.* **2015**, 284–289. [CrossRef]

47. Jones, M.O.; Kimball, J.S.; Nemani, R.R. Asynchronous Amazon forest canopy phenology indicates adaptation to both water and light availability. *Environ. Res. Lett.* **2014**, *9*, 124021. [CrossRef]

48. Joiner, J.; Yoshida, Y.; Guanter, L.; Middleton, E.M. New methods for the retrieval of chlorophyll red fluorescence from hyperspectral satellite instruments: Simulations and application to GOME-2 and SCIAMACHY. *Atmos. Meas. Tech.* **2016**, *9*, 3939–3967. [CrossRef]

49. Grace, J.; Malhi, Y.; Lloyd, J.; Mcintyre, J.; Miranda, A.; Meir, P.; Miranda, H. The use of eddy covariance to infer the net carbon dioxide uptake of Brazilian rain forest. *Glob. Chang. Biol.* **1996**, *2*, 209–217. [CrossRef]

50. Hutyra, L.R.; Munger, J.W.; Saleska, S.R.; Gottlieb, E.; Daube, B.C.; Dunn, A.L.; Amaral, D.F.; de Camargo, P.B.; Wofsy, S.C. Seasonal controls on the exchange of carbon and water in an Amazonian rain forest. *J. Geophys. Res.* **2007**, *112*, G03008. [CrossRef]

51. Canadell, J.; Jackson, R.; Ehleringer, J.; Mooney, H.A.; Sala, O.E.; Schulze, E.-D. Maximum rooting depth of vegetation types at the global scale. *Oecologia* **1996**, *108*, 583–595. [CrossRef] [PubMed]

52. Barrow, C.J. World atlas of desertification (United Nations environment programme), edited by N. Middleton and D.S.G. Thomas. Edward Arnold, London, 1992. *Land Degrad. Dev.* **1992**, *3*, 249. [CrossRef]

53. Saleska, S.R.; Wu, J.; Guan, K.; Araújo, A.; Huete, A.R.; Restrepo-Coupe, N. Dry-season greening of Amazon forests evidence from ecological studies. *Nature* **2016**, *531*, 221–224. [CrossRef] [PubMed]

54. Bi, J.; Knyazikhin, Y.; Choi, S.; Park, T.; Barichivich, J.; Ciais, P.; Fu, R.; Ganguly, S.; Hall, F.; Hilker, T.; et al. Sunlight mediated seasonality in canopy structure and photosynthetic activity of Amazonian rainforests. *Environ. Res. Lett.* **2015**, *10*, 64014. [CrossRef]

55. Wood, S.N. *Generalized Additive Models: An Introduction with R*; Chapman & Hall/CRC: Boca Raton, FL, USA, 2006.

56. Guisan, A.; Edwards, T.C.; Hastie, T. Generalized linear and generalized additive models in studies of species distributions: Setting the scene. *Ecol. Model.* **2002**, *157*, 89–100. [CrossRef]

57. Hobbie, S.E.; Nadelhoffer, K.J.; Högberg, P. A synthesis: The role of nutrients as constraints on carbon balances in boreal and arctic regions. *Plant Soil* **2002**, *242*, 163–170. [CrossRef]

58. Frankenberg, C.; Fisher, J.B.; Worden, J.; Badgley, G.; Saatchi, S.S.; Lee, J.-E.; Toon, G.C.; Butz, A.; Jung, M.; Kuze, A.; et al. New global observations of the terrestrial carbon cycle from GOSAT: Patterns of plant fluorescence with gross primary productivity. *Geophys. Res. Lett.* **2011**, *38*. [CrossRef]

59. Rossini, M.; Meroni, M.; Migliavacca, M.; Manca, G.; Cogliati, S.; Busetto, L.; Picchi, V.; Cescatti, A.; Seufert, G.; Colombo, R. High resolution field spectroscopy measurements for estimating gross ecosystem production in a rice field. *Agric. For. Meteorol.* **2010**, *150*, 1283–1296. [CrossRef]

60. Wood, J.D.; Griffis, T.J.; Baker, J.M.; Frankenberg, C.; Verma, M.; Yuen, K. Multi-scale analyses reveal robust relationships between gross primary production and solar induced fluorescence. *Geophys. Res. Lett.* **2016**, *44*, 533–541. [CrossRef]